EFFECT OF WIDTH AND TEMPERATURE OF A VERTICAL PARALLEL PLATE CHANNEL ON THE TRANSITION OF THE DEVELOPING THERMAL BOUNDARY LAYER

Ali S. Alzwayi and Manosh C. Paul[§]
Systems, Power & Energy Research Division, School of Engineering, University of Glasgow, Glasgow G12 8QQ, UK

[§]Corresponding author: Tel: +44(0)141 330 8466, Fax: +44(0)141 330 4343,
E-mail: Manosh.Paul@glasgow.ac.uk

ABSTRACT

Numerical simulations are performed to study the transition of the development of the thermal boundary layer of air along an isothermal heated plate in a large channel which is bounded by an adiabatic plate. In particular, the aim is to investigate the effects of the channel width (b) on the transition of the flow under various plate temperatures. Three different RANS based turbulent k-ε models namely standard, RNG and Realizable with an enhanced wall function are employed in the simulations. The channel width was varied from 0.04 m to 0.45 m and the numerical results of the maximum values of the flow velocity, turbulent kinetic energy were recorded along the vertical axis to examine the critical distance of the developing flow. The results show that the transition delays when the width is increased from 0.04 m to 0.08 m and particularly, the critical distance at b = 0.08 m reaches its maximum with the Grashof number of 2.8×10^{10}. However, the critical distance drops when b is increased further from 0.08 m to 0.45 m, indicating an early transition of the flow. The transition remains unaffected by the adiabatic plate when b is greater than 0.45 m. Comparisons of selected numerical results are made with available experimental data of turbulent flow and a satisfied agreement is received.

KEYWORDS: Free convection; Vertical channel; Laminar flow; Transition; Critical distance; Turbulent flow

NOMENCLATURE

A_0, A_S, C_1, C_2, $C_{1\varepsilon}$, $C_{2\varepsilon}$ and $C_{3\varepsilon}$ model constants
b channel width (m)
C_p air specific heat capacity (J/kg˚C)
g gravitational acceleration (m/s^2)
Gr Grashof number
G_k,, G_b rate of turbulent kinetic energy and buoyancy force respectively
k kinetic energy of turbulence (m^2/s^2)
L channel height (m)
$\dot{m}$ mass flow rate (kg/s)
Nu average Nusselt number
n_y , n_x number of grid nodes in the y and x directions respectively
p pressure (N/m^2)
Pr Prandtl number
q_p heat flux of the plate (W/m^2)
Ra Rayleigh number
T temperature (°C)
u, v velocity components in the x and y directions respectively (m/s)
x, y Cartesian coordinates (m)

Greek Symbols
β thermal expansion coefficient
Γ exchange coefficient for general transport defined as μ/Pr
ρ density (kg/m^3)
ν kinematic viscosity (m^2/s)
ε dissipation rate of turbulent kinetic energy (m^2/s^2)
C_μ turbulent viscosity (Pa.s)
μ dynamic viscosity coefficient (Pa.s)
μ_t turbulent molecular viscosity
σ_t constant of turbulent Prandtl number
σ_k, σ_ϵ turbulent Prandtl numbers for k and ε respectively
α thermal diffusivity (m^2/s)

Subscripts
a air
P plate
e experimental
n numerical
c critical
in inlet

1. INTRODUCTION

The fluid flow and heat transfer between two vertical plates have applications in many widely used engineering systems; for example, cooling and heating industrial and electronic equipments such as transistors, mainframe computers, plate heat exchangers, solar energy collectors, and cooling of nuclear reactor fuel elements. Therefore, over the past decades numerous numerical as well as experimental researches have been carried out to investigate the behaviour of developing heat flow inside channels made by two vertical plates. The

mechanism of the flow inside a channel can be divided into three distinct groups: free convection, forced convection and mixed convection. The movement of mass in free convection depends on the density gradient which is driven by the buoyancy force of the flow, while the flow in forced convection is driven by other external forces. On the other hand, mixed convection is driven by both free and forced convections.

Free convection has received much attention due to its wide variety of applications, e.g. by using the natural ventilation a building can reduce a conventional heating cost by 30% to 70% as reported by Liping and Angui [2004]. So, this is substantially reducing the energy consumption in a modern building. Specifically, in a vertical parallel plate channel, free convection develops when at least one of the plates is heated. But the transition of flow from laminar to turbulence usually depends on several parameters such as the properties of flow, the channel geometry, and the difference of temperature between the heated plate and the ambient condition.

In 1942 the first experimental work on the buoyancy driven convection flow in a vertical channel was done by Elenbaas [1942]. The work was done on three squares each with the dimensions of 5.95 × 5.95 cm^2, 12 × 12 cm^2 and 24× 24 cm^2 respectively. The plate thickness for the first two cases was 6 mm, while for the last one was 10 mm. The plates were isothermal and the ambient temperature was varied from 283K to 609K. The results were presented for the different ranges of inclination of the plates varying from 0˚ to 90˚ and particular attention was given to the prediction of the heat transfer coefficient of the air flow. A detailed result of the thermal characteristics of cooling by the free convection was also reported.

Numerical analysis of the turbulent convection of air in a symmetrically heated vertical parallel plate channel was done by Fedorov and Viskanta [1997]. The heated plate was tested with different values of the heat flux from 80 to 208 W/m^2. A low Reynolds number k-ε turbulent model was used in this analysis, and a finite difference numerical solution technique was employed to solve the two dimensional momentum and energy equations. The results of the local heat flux and Nusselt number distributions have been reported and compared with the experimental data of Miyamoto et al. [1986]. The results particularly indicate that the transition point moves further downstream of the channel when the turbulent intensity at the inlet is increased.

Two dimensional numerical simulations of the turbulent natural convection in a heated channel were recently performed by Said et al. [2005] and Badr et al. [2006]. The governing equations were solved by the finite volume discretization method assuming all the thermal properties of the air to be constant, except the density which was solved by the Boussinesq approximation. Specifically, the work of Badr et al. [2006] covered a wide range of thermo physical aspects of the problems as well as geometrical ratios of the model. They also compared their results with the experimental data of Miyamoto et al. [1986].

Another recent work on the natural convection in a vertical channel was reported by Ben-Mansour et al. [2006]. In the study, different inlet boundary conditions of the turbulent flow were tested; e.g. uniform inlet pressure, adiabatic inlet, and uniform inlet velocity. Numerical results of the five different k-ε turbulent models (standard, low Reynolds number k-ε Launder and Sharma [1974], low Reynolds number k-ε of Yang and Shih [1993], Renormalization Group (RNG) k-ε, and Reynolds stress) were presented. Steady state two-dimensional numerical model was developed and the results showed that the thermal field, which was

obtained by the low Reynolds number *k-ε* model of Yang and Shih [1993] with a uniform pressure inlet condition, was very close to the experimental results of Miyamoto et al. [1986]. Experimental and numerical work was also done by Yilmaz and Fraser [2007] on the turbulent free convection boundary layer in a vertical parallel plate channel with asymmetric heating.

As evident from the summary of the literature survey, the natural convection between two vertical plates has extensively been studied by numerous researchers, and several published papers presented the main characteristics of flow with different boundary conditions. The majority of these papers presented the results of velocity, temperature and turbulence parameters in the vertical direction of the flow; but none of these papers provides information about the transition of the flow inside the channel and importantly how the transition is affected by the merging of the two growing boundary layers inside the channel. In this study the effect of the plate and air temperatures on the transition are investigated. In addition, particular attention is given to the effect of the range of channel width on the transition stage.

2. MODEL GEOMETRY

The channel is formed by the two vertical plates with length *L*, and the distance between the plates is denoted by *b*. The wall on the left side is isothermal, while the other is adiabatic. The numerical simulations are considered to be two dimensional free-convection and steady state. The air is chosen to be the test fluid. The model geometry along with the Cartesian coordinate system is shown in Figure 1. For the comparison with the experimental data, the model geometry is studied under the same physical dimensions of the experimental model of Yilmaz and Fraser [2007], where L = 3.0 m and b = 0.1 m.

3. MATHEMATICAL FORMULATION

3.1 Governing Equations For a two dimensional incompressible fluid flow the conservation equations of momentum, mass and energy are written in the following forms as reported in Markatos and Pericleous [1984] and Bacharoudis et al. [2007].

$$\frac{\partial(\rho u)}{\partial x}+\frac{\partial(\rho v)}{\partial y}=0 \tag{1}$$

$$\frac{\partial(\rho uu)}{\partial x}+\frac{\partial(\rho uv)}{\partial y}=-\frac{\partial P}{\partial x}+\frac{\partial}{\partial x}\left(\mu\frac{\partial u}{\partial x}\right)+\frac{\partial}{\partial y}\left(\mu\frac{\partial u}{\partial y}\right) \tag{2}$$

$$\frac{\partial(\rho vu)}{\partial x}+\frac{\partial(\rho vv)}{\partial y}=-\frac{\partial P}{\partial y}+\frac{\partial}{\partial x}\left(\mu\frac{\partial v}{\partial x}\right)+\frac{\partial}{\partial y}\left(\mu\frac{\partial v}{\partial y}\right)+g(\rho-\rho_0) \tag{3}$$

$$\frac{\partial(\rho uT)}{\partial x}+\frac{\partial(\rho vT)}{\partial y}=\frac{\partial}{\partial x}\left(\Gamma\frac{\partial T}{\partial x}\right)+\frac{\partial}{\partial y}\left(\Gamma\frac{\partial T}{\partial y}\right) \tag{4}$$

The conservation equations (1–4) are solved directly for the natural convection flow in the laminar region, while in the turbulent region both the Γ and μ terms are replaced by the effective values, Γ_{eff} and μ_{eff}, as presented in Nicholas and Markatos [1978] and Bacharoudis et al. [2007], and defined by $\mu_{eff} = \mu + \mu_t$ and $\Gamma_{eff} = \mu/Pr + \mu_t/\sigma_t$ respectively. In this study a comparison among the three different *k-ε* models (standard, RNG and Realizable) are made. Note that the major differences among these models are the ways to determine the turbulent viscosity μ_t, the turbulent dissipations energy ε, and the turbulent kinetic energy k, described below.

3.2 Standard *k-ε* Model The standard *k-ε* model was initially proposed by Launder and Spalding [1972] and based on the two terms: the dissipation rate ε, and the turbulent kinetic

energy *k*. The model transport equation for ε is obtained by employing physical reasoning, while the turbulent kinetic energy *k* is derived from an exact equation by assuming that the effect of the molecular viscosity of the flow is negligible and the flow is fully developed. The distribution of the turbulent kinetic energy *k* and the rate of dissipation ε can be determined from the following equations:

$$\frac{\partial(\rho uk)}{\partial x}+\frac{\partial(\rho vk)}{\partial y}=\frac{\partial}{\partial x}\left[\left(\mu+\frac{\mu_t}{\sigma_k}\right)\frac{\partial k}{\partial x}\right]+\frac{\partial}{\partial y}\left[\left(\mu+\frac{\mu_t}{\sigma_k}\right)\frac{\partial k}{\partial y}\right]+G_k+G_b-\rho\varepsilon \quad (5)$$

$$\frac{\partial(\rho u\varepsilon)}{\partial x}+\frac{\partial(\rho v\varepsilon)}{\partial y}=\frac{\partial}{\partial x}\left[\left(\mu+\frac{\mu_t}{\sigma_\varepsilon}\right)\frac{\partial \varepsilon}{\partial x}\right]+\frac{\partial}{\partial y}\left[\left(\mu+\frac{\mu_t}{\sigma_\varepsilon}\right)\frac{\partial \varepsilon}{\partial y}\right]+G_{1\varepsilon}\frac{\varepsilon}{k}(G_k+G_{3\varepsilon}G_b)-C_{2\varepsilon}\rho\frac{\varepsilon^2}{k} \quad (6)$$

where

σ_k , σ_ε are the Prandtl numbers for *k* and ε, taken as 1.0 and 1.3, respectively.

G_k is the rate of the kinetic energy determined from $\mu_t\left(\frac{\partial u_i}{\partial x_j}+\frac{\partial u_j}{\partial x_i}\right)\frac{\partial u_i}{\partial x_j}-\frac{2}{3}\rho k\delta_{ij}\frac{\partial u_i}{\partial x_j}$.

δ_{ij} is the Kronecker delta (δ_{ij} =1.0 if $i=j$ and δ_{ij} =0.0 if $i\neq j$) .

G_b is the buoyancy force $= g_i\beta\frac{\mu_t}{\sigma_t}\frac{\partial T}{\partial x_i}$ and μ_t is the turbulent viscosity $= \rho C_\mu k^2/\varepsilon$.

The adjustable constants are $C_{1\varepsilon}$ = 1.44, $C_{2\varepsilon}$ = 1.92, $C_{3\varepsilon}$ = 1.0 and C_μ = 0.09.

3.3 RNG *k*-ε Model The renormalization group (RNG) was derived by Yakhot et al. [1992] with an extensive analysis of the eddy viscosity model. The RNG *k*-ε model carries an additional factor in the turbulent dissipation energy (ε) equation, which leads to improving the accuracy of strain in the flow. The RNG *k*-ε model has a similar form of the kinetic and dissipation energy equations compared with the standard model:

$$\frac{\partial(\rho uk)}{\partial x}+\frac{\partial(\rho vk)}{\partial y}=\frac{\partial}{\partial x}\left[\alpha_k\mu_{eff}\frac{\partial k}{\partial x}\right]+\frac{\partial}{\partial y}\left[\alpha_k\mu_{eff}\frac{\partial k}{\partial y}\right]+G_k+G_b-\rho\varepsilon \quad (7)$$

$$\frac{\partial(\rho u\varepsilon)}{\partial x}+\frac{\partial(\rho v\varepsilon)}{\partial y}=\frac{\partial}{\partial x}\left[\alpha_\varepsilon\mu_{eff}\frac{\partial \varepsilon}{\partial x}\right]+\frac{\partial}{\partial y}\left[\alpha_\varepsilon\mu_{eff}\frac{\partial \varepsilon}{\partial y}\right]+C_{1\varepsilon}\frac{\varepsilon}{k}(G_k+C_{3\varepsilon}C_b)-C_{2\varepsilon}\rho\frac{\varepsilon^2}{k}-R_\varepsilon \quad (8)$$

where $\alpha_k = \alpha_\varepsilon \approx 1.393$ are the inverse effective Prandtl numbers, and R_ε is an additional term related to the mean strain and turbulence quantities. The models constant are $C_{1\varepsilon}$ = 1.42, $C_{2\varepsilon}$ = 1.68 and $C_{3\varepsilon}$ = 1.0.

The turbulent viscosity (μ) is determined from $\mu = \rho C_\mu k^2/\varepsilon$ with C_μ = 0.0845, whereas the effective viscosity is calculate by $v_v = \mu_{eff}/\mu$, where $d\left(\frac{\rho^2 k}{\sqrt{\varepsilon\mu}}\right) = 1.72\frac{v_v}{\sqrt{({v_v}^3-1+C_v)}}dv_v$ and $C_v \approx 100$.

3.4 Realizable *k*-ε Model Realizable *k*-ε model was proposed by Shih et al. [1995], which was derived based on the dynamic equations of the mean square fluctuation at a large range of Reynolds number, so the model has an ability to control the Reynolds stresses. The conservation equations are

$$\frac{\partial(\rho uk)}{\partial x}+\frac{\partial(\rho vk)}{\partial y}=\left[\left(\mu+\frac{\mu_t}{\sigma_k}\right)\frac{\partial k}{\partial x}\right]+\frac{\partial}{\partial y}\left[\left(\mu+\frac{\mu_t}{\sigma_k}\right)\frac{\partial k}{\partial y}\right]+G_k+G_b-\rho\varepsilon \quad (9)$$

$$\frac{\partial(\rho u\varepsilon)}{\partial x}+\frac{\partial(\rho v\varepsilon)}{\partial y}=\frac{\partial}{\partial x}\left[\left(\mu+\frac{\mu_t}{\sigma_\varepsilon}\right)\frac{\partial \varepsilon}{\partial x}\right]+\frac{\partial}{\partial y}\left[\left(\mu+\frac{\mu_t}{\sigma_\varepsilon}\right)\frac{\partial \varepsilon}{\partial y}\right]+\rho C_1 S_\varepsilon-\rho C_2\frac{\varepsilon^2}{\varepsilon+\sqrt{\nu\varepsilon}}+G_{1\varepsilon}\frac{\varepsilon}{k}C_{3\varepsilon}G_b \quad (10)$$

where, $C_1 = \max[0.43, \eta/(\eta+5)]$ and $\eta = Sk/\varepsilon$. A new formula is used to compute the eddy viscosity as reported by Shih et al. [1995]; and $\mu_t = \frac{\rho k^2}{\varepsilon}\left(A_0+A_S\frac{kU^*}{\varepsilon}\right)^{-1}$ where A_0 and A_S are the model constants given as A_0 = 4.04 and $A_s = \sqrt{(6\cos\emptyset)}$ respectively with $\emptyset = 1/3\cos^{-1}\left(\sqrt{6}W\right)$. The formulations for U^* and *W* depend on the angular velocity, and more details can be found in Shih et al. [1995]. Note that the model constants in this model are $C_{1\varepsilon}$ = 1.44, C_2 = 1.9, $C_{3\varepsilon}$ = 1.0, σ_k = 1.0 and σ_ε = 1.2.

4. BOUNDARY CONDITIONS FOR THE MODEL

At the inlet, ambient temperature and pressure conditions are applied so that the air velocity is accelerated from the rest to the induced velocity *v*. Moreover, in the case of natural transition the flow is expected to develop from the laminar stage, therefore the turbulent kinetic energy (k) and its dissipation (ε) are set to zero at the inlet. A uniform temperature is imposed at the heated plate of the channel while the other plate is adiabatic. At the outlet, the static gauge pressure is set to zero and the solver extrapolates the other flow and turbulent quantities from the interior domain.

No slip boundary condition is imposed on the velocity components at the walls, where $u_i = 0$, for $0 \leq y \leq L$, $x = 0$ and $x = b$.

The thermal boundary conditions for the heated and the adiabatic plate are defined as
$T = Tp$, for $0 \leq y \leq L$, $x = 0$ and
$\frac{\P T}{\P x} = 0$, for $0 \leq y \leq L$, $x = b$.

Moreover, the turbulent kinetic energy vanishes at the wall, so
$k = 0$, for $0 \leq y \leq L$, $x = 0$ and $x = b$.

It is important to note here that when a comparison with the experimental data of Yilmaz and Fraser [2007] is presented, the model is studied under the experimental conditions where the inlet temperature is assumed to be 23°C. The isothermal conditions for the heated plate is set at the temperature of 100°C, and the turbulent intensity at the inlet is measured to be 13%. Moreover, the distributions of the characteristics of the flow have large gradients near the wall so an enhanced wall function is used in the boundary.

5. NUMERICAL TECHNIQUES

The finite volume method is used to discretise the governing equations with the second order upwind scheme to solve the discretised equations, where the unknown quantities at the cell faces are computed by using a multidimensional linear reconstruction approach described in Barth and Jespersen [1989] to achieve higher order at the cell faces through a Taylor series expansion of the cell centered solution about the cell centroid.

The SIMPLE algorithm of Patankar [1980] is then employed to solve the pressure based equation which is derived from the momentum and continuity equations such that the velocity and pressure fields are coupled to each other and solved by adopting an iterative solution strategy. In this algorithm, the discretised momentum equations are initially solved by using an assumed pressure field (p^*) to yield the velocity solutions (u^*, v^*). A correction to the pressure (p'), which is the difference between the actual and assumed pressures, is then applied to achieve a better approximation of the pressure field using $p = p' + p^*$. Similarly, the velocity components are corrected to get (u, v); and then the discretised equations of a scalar quantity e. g. the energy (T), turbulent energy (k) and its dissipation rate (ε) are solved using the most updated results of (u, v, p). All these equations are solved sequentially and iteratively using Fluent 6.3; and the final numerical solutions are achieved when the residuals of the continuity and velocity components become less than 10^{-6}. The residual of the energy, turbulent kinetic energy and its dissipation is reduced to 10^{-8} to avoid any sensitivity to the solutions of the turbulent fluctuating components.

6. GRID RESOLUTION TEST

Mesh dependence study was initially carried out on the Realizable turbulent model to find out a suitable combination of the grid sizes which will be applicable to resolve the flow inside the channel. This mesh dependence study was performed by changing the total number of grid nodes in both the vertical (n_y) and horizontal (n_x) directions by using six different grid resolutions e.g. 22 × 220, 30 × 370, 120 × 370, 200 × 370, 300 × 370 and 200 × 400. Non-uniform structured mesh was generated in the channel with a fine resolution of grid clustered near the inlet and walls by using the mesh-successive ratios of 1.008 and 1.01 respectively.

Figure 2 shows the results of the heated air velocity (v), turbulent kinetic energy (k) and air temperature in three different vertical locations, y = 0.09 m, 1.5 m and 3.0 m. As can be seen both the coarse (especially in the horizontal direction) grids, 22 × 220 and 30 × 370, provide somehow satisfactory results for the velocity and temperature fields, but severely overestimate the turbulent kinetic energy production inside the channel. The next four finer grids, 120 × 370, 200 × 370, 300 × 370 and 200 × 400, produce most satisfactory results since the differences found among the results are very small indeed and almost negligible. Therefore, either of these four grids could be used, however to avoid any undesirable discrepancies in the numerical results and at the same time to save the computational time the grid size of 200 × 370 is chosen to perform all the numerical simulations.

7. ASSESSMENT OF THE DIFFERENT TURBULENT MODELS

Figure 3 (a) presents the distribution of the temperature of air at the outlet of the channel predicted by the three turbulent models. A comparison with the experimental data of Yilmaz and Fraser [2007] is made; and it is found that the Realizable turbulent model gave the best predicted results compared to the RNG and standard models.

The velocity profiles are presented in Figure 3 (b) at the two different vertical locations, 0.09 m and 2.94 m. The velocity at y = 0.09 m shows a symmetric profile, as this location is very close to the inlet, so the effect of the adiabatic plate on the velocity is negligible. But, this was not the case in the experimental data, which show some asymmetries near the adiabatic plate close to x = 0.09 m, and surprisingly, none of the simulations accurately predicts this behaviour and the velocity profile is approximately smooth and flat in the centre of the channel. With an increase in the vertical distance of the heated plate, i.e. at y = 2.94 m, the peak of the velocity profile appears beside the heated plate due to the fact that the buoyancy force beside the heated wall becomes very large and has a profound effect on the flow development near the wall.

Over all, comparing among the three different numerical models, the velocity profile close to the inlet (y = 0.09 m) by the RNG turbulent model shows a very good agreement with the experimental data, especially within the range $0 \leq x \leq 0.08$ m. However, near the outlet of the channel, e. g. at y = 2.94 m, the Realizable turbulent model gives the numerical results which are close to the experimental data.

The numerical prediction of the turbulent kinetic energy shown in Figure 3 (c) is lower than the experimental data. At y = 2.94 m the turbulent kinetic energy reaches its maximum at the centre of the channel, which has an agreement with the experimental data of Yilmaz and

Fraser [2007]. And, particularly, the Realizable model predictions are more close to the experiment than the other two models.

Over all, seeing all the results in Figure 3 and by employing the enhanced wall function with the three different turbulent models (standard, RNG and Realizable), the percentages of error to calculate the velocity near the outlet are found to be 8.97%, 9.7% and 6.3% respectively. The same comparison can be made for the outlet temperature, which are 1.75%, 1.73% and 1.55% respectively. Therefore, it is clear that the enhanced wall function is capable of predicting the distribution of the outlet temperature with all the models of the turbulent flow. However, comparatively the Realizable turbulent model performed best, therefore it is selected to perform all the other numerical simulations for studying transition, and the results are presented in the following sections.

8. EFFECT OF PLATE TEMPREATURE ON THE TRANSITION STAGE

The transition stage of the developing flow inside the channel is determined by the numerical results of the maximum values of the velocity and turbulent kinetic energy, where the maximum quantities are determined by using $f_{\max}(y) = \underset{x\min \le x \le x\max}{Max} f(x,y)$, where f is a generic function, and plotted along the vertical axis y. Figure 4 (a) and (b) shows the production of the maximum velocity and kinetic energy of the heated air respectively where the channel width is fixed at b = 0.1m. As we can see, with an increase in the plate temperature (Tp) from 50˚C to 100˚C, generally the transition of the flow from the laminar to turbulent stage starts early. This can be seen in Figure 5 where the critical distance on the plate, derived from the maximum velocity and kinetic energy, is presented. More specifically, the results show that at a constant air temperature e. g. Ta = 15˚C with an increase in the plate temperature by 100%, e. g. from 50˚C to 100˚C, the critical distance of the plate droops by 16.4%. The range of the Grashof number at the transition point is also calculated, which varies from $Gr = 1.03\times10^{10}$ for Tp = 100˚C to $Gr = 1.22\times10^{10}$ for Tp = 50˚C.

9. EFFECT OF CHANNEL WIDTH ON THE TRANSITION STAGE

Numerical results of the velocity, turbulent kinetic energy and local heat flux are presented in this section to investigate the effects of the width of the channel on the process of transition occurring inside the channel. The heated plate of the channel is kept as isothermal at 70°C with the inlet air temperature of 15°C, but the width of the channel is varied from 0.04 m to 0.45 m to study the transition effects.

To avoid any ambiguity in presenting the numerical results, the profiles are divided into two groups: the first group presents the results of the width from b = 0.04 m to b = 0.1 m; whereas the second one from b = 0.15 m to b = 0.45 m. Figure 6 (a) shows that the maximum velocity for the width b = 0.04 m to 0.1 m reaches its maximum at the transition point, then it starts to drop slightly and after that the growth becomes approximately constant towards the downstream of the channel. For the turbulent kinetic energy in Figure 6 (b), its value is initially zero at the inlet and within the laminar region of the channel. But the kinetic energy grows rapidly in the region where the transition begins, and the growth remains steady within the whole transition region, followed by a sharp increase in the region of the turbulent flow in the most cases. Specifically, for a small width of the channel, e.g. at b = 0.04 m and 0.05 m, the kinetic energy reaches its peak approximately at $y \approx 1.5$ m, while for b = 0.06 m and 0.10 m the location of peaks becomes later at y = 1.8 m and 2.4 m respectively.

In the second group, the results in Figure 6 (c) show that the growth of the velocity profile at b = 0.15 m to 0.45 m is gradual in the laminar flow region, but just after the transition point it drops slightly and then increases again towards the downstream because of the presence of turbulence. The nature of the growth in the kinetic energy in Figure 6 (d) for b = 0.15 m and 0.2 m remains quite similar, e.g. rapid rise at the beginning of the transition and then steady within the transition region, and finally sharp rise at the downstream. However, the transition region found for b = 0.30 m and 0.45 m is relatively small compared to the other cases, and the growth of the kinetic energy becomes similar to that found in the one-heated plate case.

Figure 7 (A) shows the contour plots of the turbulent kinetic energy inside the channel. As can be seen the turbulent kinetic energy reaches its maximum at the outlet of channel for the width $b \geq 0.08$ m. But for $b \leq 0.06$ m it reaches its maximum in the range 1.5 m $\leq y \leq$ 2.5 m. The distributions of the turbulent intensity are shown in Figure 7 (B), which show some interesting features of the growth of turbulence in the channel. Particularly, when the width is reduced, the intensity also grows on the right side of the channel where the adiabatic plate is located.

Additionally, as seen in Figure 7 (A), the distribution of the kinetic energy as well as the intensity is complicated, especially in the range of the channel width smaller than 0.20 m, where the kinetic energy grows on the both sides of the channel. So, to understand the growth of the kinetic energy in more details within the channel the results are divided into two regions and presented in Figure 8, where the maximum kinetic energy is first calculated in the range of $0 \leq x \leq b/2$ to look into the growth near the heated plate on the left hand side of the channel and plotted in frames (a) and (c). Whereas the maximum of the same is recorded in the rage of $b/2 \leq x \leq b$ to particularly focus on the turbulence production near the adiabatic plate and shown in frames (b) and (d).

As evidenced in Figure 8 (a), the kinetic energy on the heated plate grows early with dropping the width of the channel from b = 0.04 m to b = 0.10 m. Although the right side plate of the channel is kept as adiabatic, the kinetic energy still grows on it especially for the channel width b = 0.04 m to 0.20 m, see Figure 8 (b) and (d). But, for a large channel width e.g. b = 0.30 m and 0.45 m, in Figure 8 (d), the growth of the kinetic energy on the right side can be ignored since the maximum distribution of the kinetic energy is found inside the channel. Importantly, Figure 6 (d) is similar to the distribution of the kinetic energy on the left side of the channel as shown in Figure 8 (c), so its distribution is more dependent on the heated plate and the velocity distribution.

Since the peak of temperature and velocity distribution from the heated plate can be considered to be a starting point of the transition stage according to Katoh et al. [1991], where the location of a minimum point of the local heat flux should also correspond to the transition point, the three different parameters of the heated air such as the velocity, turbulent kinetic energy and local heat flux are used to predict the transition point inside the channel with different values of the width. The values of the critical distance at the transition point are derived from the velocity and the kinetic energy already presented in Figure 6 and now summarised in Figure 9.

Figure 9 shows that the transition points predicted by the turbulent kinetic energy are very close to those estimated by the velocity distribution in all the cases. In addition, for a large channel width $b \geq 0.1$ m the local heat flux also predicts the critical distance that agrees well

with other two results. However, for a small channel width e.g. b = 0.04 m to 0.08 m Figure 9 shows that the local heat flux reaches its minimum further upstream of the channel and does not agree with the predictions of the velocity and the turbulent kinetic energy. The possible reason for that is that both the thermal and the thickness of the boundary layer increase sharply in the turbulent flow compared to the laminar flow due to the effects of the buoyancy force on the heated plate. Additionally, at a small width of the channel there is not enough space for the boundary layer to grow fully which would eventually carry the heat from the heated plate; so as a consequence, the specific heat transfer of the air reaches its maximum temperature early.

Moreover, Figure 9 also shows that the location of the transition point shifts to a higher distance towards the downstream of the channel when the channel width is increased from b = 0.04 m to 0.08 m. And, particularly, at b = 0.08 m the critical distance reaches its maximum of 1.53 m in the middle of the channel, where the Grashof number calculated as a function of this critical distance of the velocity is 2.8×10^{10} (Figure 10). However, as seen, the transition occurs early when the channel width is increased from b = 0.10 m to 0.45 m, and the critical distance at the channel width of 0.45 m becomes similar to that obtained by the one vertical heated plate since the effect from the adiabatic plate at a far distance is negligible. Importantly, the Grashof number (Figure 10) at the critical distance for Ta = 15°C and b = 0.45 m is estimated to be 2.27×10^{9} and 1.17×10^{9} for the one plate case, which has a close agreement to $\approx10^{9}$ obtained by Bejan [1995] in the free convection flow on an isothermal vertical plate.

10. EFFECTS OF WIDTH ON THE THERMAL BOUNDARY LAYER

To investigate the effects of the width of the channel on the distributions of the thermal boundary layer of the heated air developing inside the channel as well as on its thickness, results of the air temperature, velocity and turbulent kinetic energy are reported in the horizontal direction (x) at different vertical locations; near the entrance (at y = 0.5 m), outlet, middle of the channel (at y = 1.5 m), and the critical location (at $y = Lc$). The width of the channel is varied from b = 0.04 m to b = 0.2 m.

The axial dimensionless temperature profiles which are plotted in Figure 11 at different heights show a general trend i.e. the temperature besides the isothermal plate is maximum which then drops to the adiabatic plate on the right. The profiles also show a gradual increase in the air temperature from the inlet towards the downstream of the channel in all the cases due to the growth of the thermal boundary layer along the channel. But the boundary layer growth is affected by the channel width. Particularly, as can be seen in frames (a-e), when b is reduced from 0.2 m to 0.04 m, the outlet temperature at the adiabatic plate increases. The thickness of this developing thermal boundary layer can now be estimated by using the relationship, $\delta \approx y/Ra^{1/5}$, available in Armfield et al. [2007] and compared with their predictions. Under the same thermal conditions they showed that the thickness of the fully developed turbulent thermal boundary layer on an isothermally heated vertical plate is approximately 0.21 m. Whereas, in Figure 11 (f) for b = 0.20 m, the thickness of the thermal boundary layer at the outlet section is calculated to be 0.19 m which somehow shows a good level of agreement with that of Armfield et al. [2007].

The variation of the turbulent mean velocity across the channel is plotted in Figure 12 for the same channel width. As can be seen the velocity at the inlet increases gradually when the channel width b is reduced. Moreover, in all the cases the peak of the velocity profile appears

beside the heated plate (on the left side) as expected; but when b is increased, the velocity peaks become sharp and move towards the heated plated, indicating a rapid acceleration of the air flow near the heated plate. However, the magnitude of the velocity drops first slowly from their peaks and then rapidly towards the adiabatic surface on the right side, clearly seen in Figure 12 (a–d) for b = 0.04 m to 0.10 m. In contrast, the velocity profiles for b = 0.15 m and 0.20 m, and particularly at the outlet, show a sharp drop to the adiabatic plate and remain almost flat at the critical distance within a wide range of the channel section. This characteristic behaviour of the velocity profiles predicted inside the channel has also a good agreement with the experimental data of Katoh et al. [1991].

Additionally, the peak velocity at the transition point for the width of 0.04 m to 0.10 m is higher than that at the outlet section, in Figure 12 (a–d); this is possibly due to the enhanced turbulent mixing within the relatively small width of the channel. Whereas, for b = 0.15 m and 0.20 m, in Figure 12 (e–f), the peak velocity at the outlet becomes higher than the transition section; and these issues are further explored in more details in Figure 13 where the peak velocity at the transition point and at the outlet section of the channel is compared. The results show that with an increase in the width of the channel from 0.04 m the peak velocity at the outlet section of the channel initially drops and becomes less than that of the critical distance. However, after about 0.1 m the peak velocity at the outlet increases slightly and becomes larger than the transition stage when $b > 0.12$ m.

The distributions of the turbulent kinetic energy are presented in Figure 14. The results show that the prediction profile of the turbulent kinetic energy for the channel width b = 0.04 m to 0.08 m is larger at the middle of the channel (y = 1.5 m) than that of the outlet section especially near the heated plate. Moreover, the kinetic energy for b = 0.04 m and 0.06 m reaches its peak near the adiabatic plate as shown in Figure 14 (a–b). Whilst in the rest of channels, when width $b \geq 0.08$ m, the turbulent kinetic energy at the outlet section reaches its peak approximately at the middle of the channel, i.e. at $x = b/2$.

11. CONCLUSION

Numerical results of the transition inside a channel have been presented in this paper giving a particular attention to the effects of the channel width on the distributions of the velocity, kinetic energy, temperature and plate heat flux. The results in the turbulent flow have been compared satisfactorily with the experimental data among with the three different turbulent models namely the standard, RNG and Realizable k-ε. Importantly, an enhanced wall function has been applied to the surfaces to account the developing boundary layers, and the results showed that the Realizable turbulent model gave the least error compared to the other two models.

To present the effects of the thermal conditions on the transition stage we initially fixed the channel width at b = 0.10 m but varied the plate temperature. The results showed that an increase in the plate temperature caused an early transition of the flow since the critical distance dropped. The critical distance estimated from the distributions of the flow velocity and the turbulent kinetic energy along the vertical channel agree very well.

Additionally, we have found that the width of the channel has a major effect on the transition. For example, with an increase in the channel width from b = 0.04m to 0.08m the transition delays, and particularly the critical distance reaches its maximum at b = 0.08 m with the Grashof number of 2.8×10^{10}. On the other hand, the transition occurs early when the

channel width is increased from 0.08m, and the critical distance at b = 0.45m becomes similar to that of the single plate case.

Moreover, for $b \geq 0.10$ m the values of the critical distance, which are a function in the local heat flux, are very close to the distribution of the velocity and kinetic energy; but for the small width e.g. when $b \leq 0.08$ m, the local heat flux reaches its minimum in a location which is far away from the critical distance obtained by the velocity and turbulent kinetic energy.

REFERENCES

Armfield, S, W. Patterson, J, C. and Lin, W. [2007], Scaling investigation of the natural convection boundary layer on an evenly heated plate, *Int. Journal of Heat and Mass Transfer,* Vol. 50, pp 1592-1602.

Bacharoudis, E. Vrachopoulos, M. Koukou, M, K. Margaris, D. Filios, A, E. and Mavrommatis, S, A. [2007], Study of the natural convection phenomena inside a wall solar chimney with one wall adiabatic and one wall under a heat flux, *Applied Thermal Engineering*, Vol. 27, pp 2266-2275.

Barth, T. J. and Jespesen, D. [1989], The design and application of upwind schemes on unstructured meshes, Technical report AIAA-89-0366, *Aerospace sciences meeting*, Reno, Nevada.

Badr, H, M. Habib, M, A. and Anwar, S. [2006], Turbulent natural convection in vertical parallel-plate channels, *Heat Mass Transfer*, Vol. 43, pp 73-84.

Bejan, A. [1995], *Convection Heat Transfer*, Second edition, Wiley, New York.

Ben-Mansour, R. Habib, M, A. Badr, H, M. and Anwar, S. [2006], Comparison of different turbulent models and flow boundary conditions in predicting turbulent natural convection in a vertical channel with isoflux plates, *The Arabian Journal for Science and Engineering*, Vol. 23, pp 191-218.

Elenbaas, W. [1942], Heat dissipation of parallel plates by free convection, *Physica IX* 9, pp 1-28.

Fedorov, A, G. and Viskanta, R. [1997], Turbulent natural convection heat transfer in an asymmetrically heated, vertical parallel-plate channel, *Int. J. Heat Mass Transfer*, Vol. 40, pp 3849-3860.

Katoh, Y. Miyamoto, M. Kurima, J. and Kaneyasu, S. [1991], Turbulent free convection heat transfer from vertical parallel plates, *JSME International Journal*, Vol. 34, pp 496-501

Launder, B, E. and Spalding, D, B. [1972], *Lectures in mathematical models of turbulence*, Academic Press, London, England.

Launder, B, E. and Sharma, B, I. [1974], Application of the energy-dissipation model of turbulence to the calculation of flow near a spinning disc, *Letters in Heat and Mass Transfer*, Vol. 1, pp 131-138.

Liping, W. and Angui, L., 2004. A numerical study of vertical solar chimney for enhancing stack ventilation in buildings , *The 21st Conference on Passive and Low Energy Architecture Eindhoven,* The Netherlands, pp 1-5.

Markatos, N, C. and Pericleous, K, A. [1984], Laminar and turbulent natural convection in an enclosed cavity, *Int. J. Heat Mass Transfer*, Vol. 27, pp 755-772.

Miyamoto, M. Katoh, Y. Kurima, J. and Saki, H. [1986], Turbulent free convection heat transfer from vertical parallel plates, *proceeding of the International Heat Transfer, conference 8th*. Vol. 4, pp 1593-1598.

Nicholas, A, S. and Markatos, C, G. [1978], Transient flow and heat transfer of liquid sodium coolant in the outlet plenum of a fast nuclear reactor, *International Journal Heat Mass Transfer*, Vol. 21, pp 1565-1579.

Patankar, S, V. [1980], *Numerical Heat Transfer and Fluid Flow*, New York.

Said, S, A, M. Habib, M, A. Badr, H, M. and Anwar, S. [2005], Turbulent natural convection between inclined isothermal plates, *Computers and Fluids*, Vol. 34, pp 1025-1039.

Shih, T, H. Liou, W, W. Shabbir, A. Yang, Z. and Zhu, J. [1995], A new k-ε eddy viscosity model for high Reynolds number turbulent flows, *Computers and Fluids*, Vol. 24, pp 227-238.

Yakhot, V. Orszag, A, S. Thangam, S. and Speziale, G. C. [1992], Development of turbulence models for shear flows by a double expansion technique, *Physics of Fluids*, Vol. 4, pp 1510-1521.

Yang, Z. and Shih, T, H. [1993], New Time Scale Based $k-\varepsilon$ Model for Near-Wall Turbulence, *American Institute of Aeronautics and Astronautics Journal*, Vol. 31, pp 1191-1198.

Yilmaz, T. and Fraser, S, M. [2007], Turbulent natural convection in a vertical parallel-plate channel with asymmetric heating, *Int. Journal of Heat and Mass Transfer*, Vol. 50, pp 2612-2623.

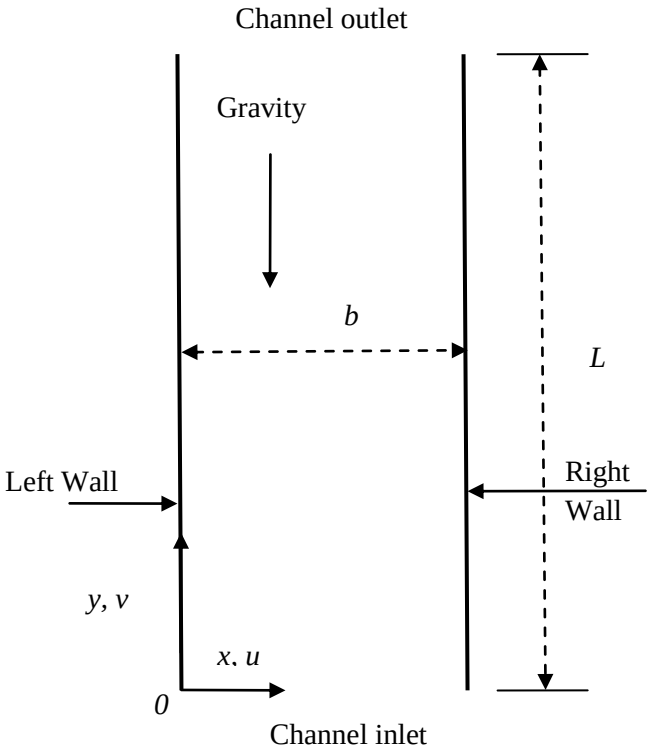

Figure 1. The vertical parallel plate channel.

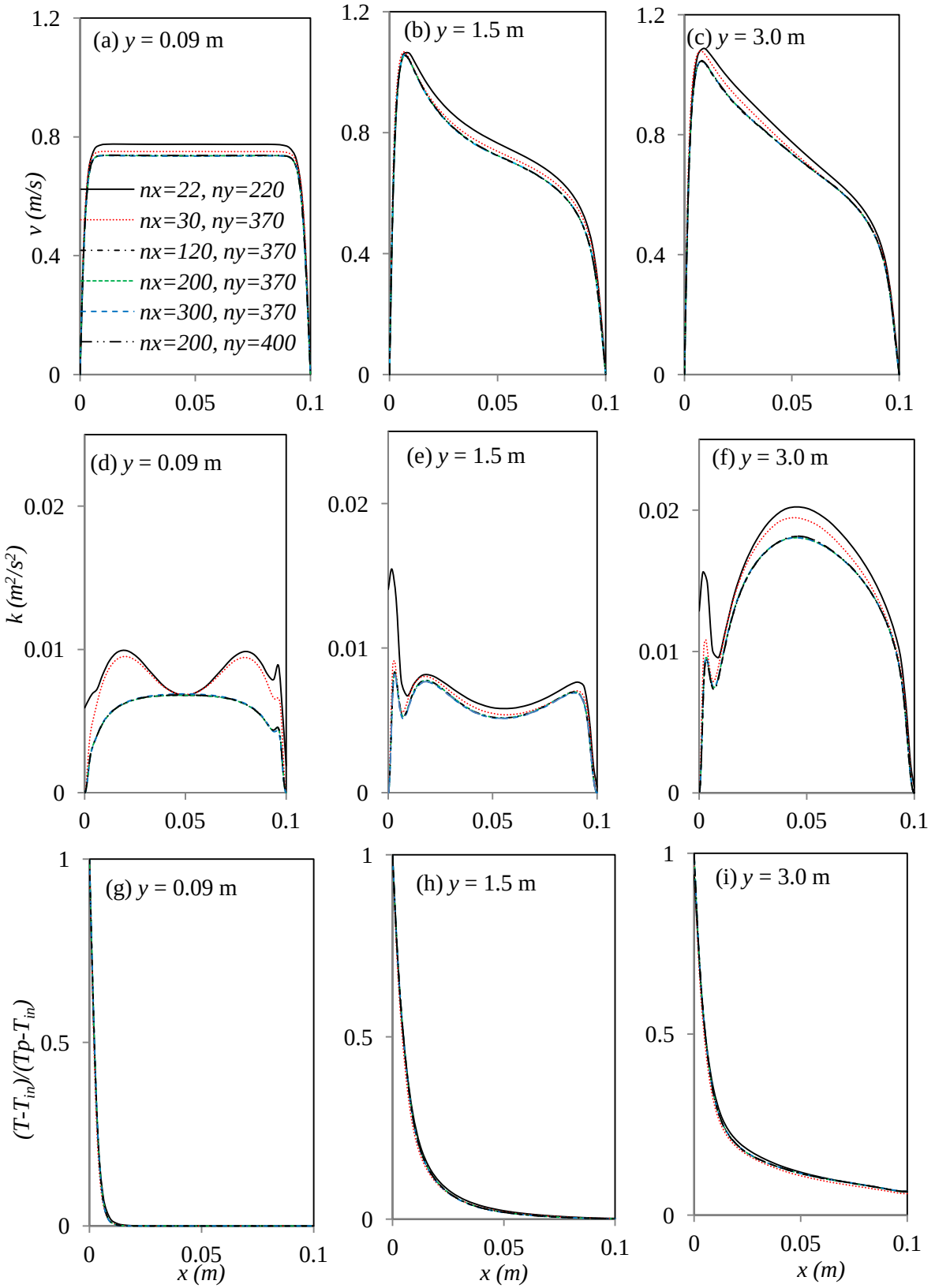

Figure 2. Mesh dependence test showing the results of velocity, turbulent kinetic energy and air temperature at different locations along the channel.

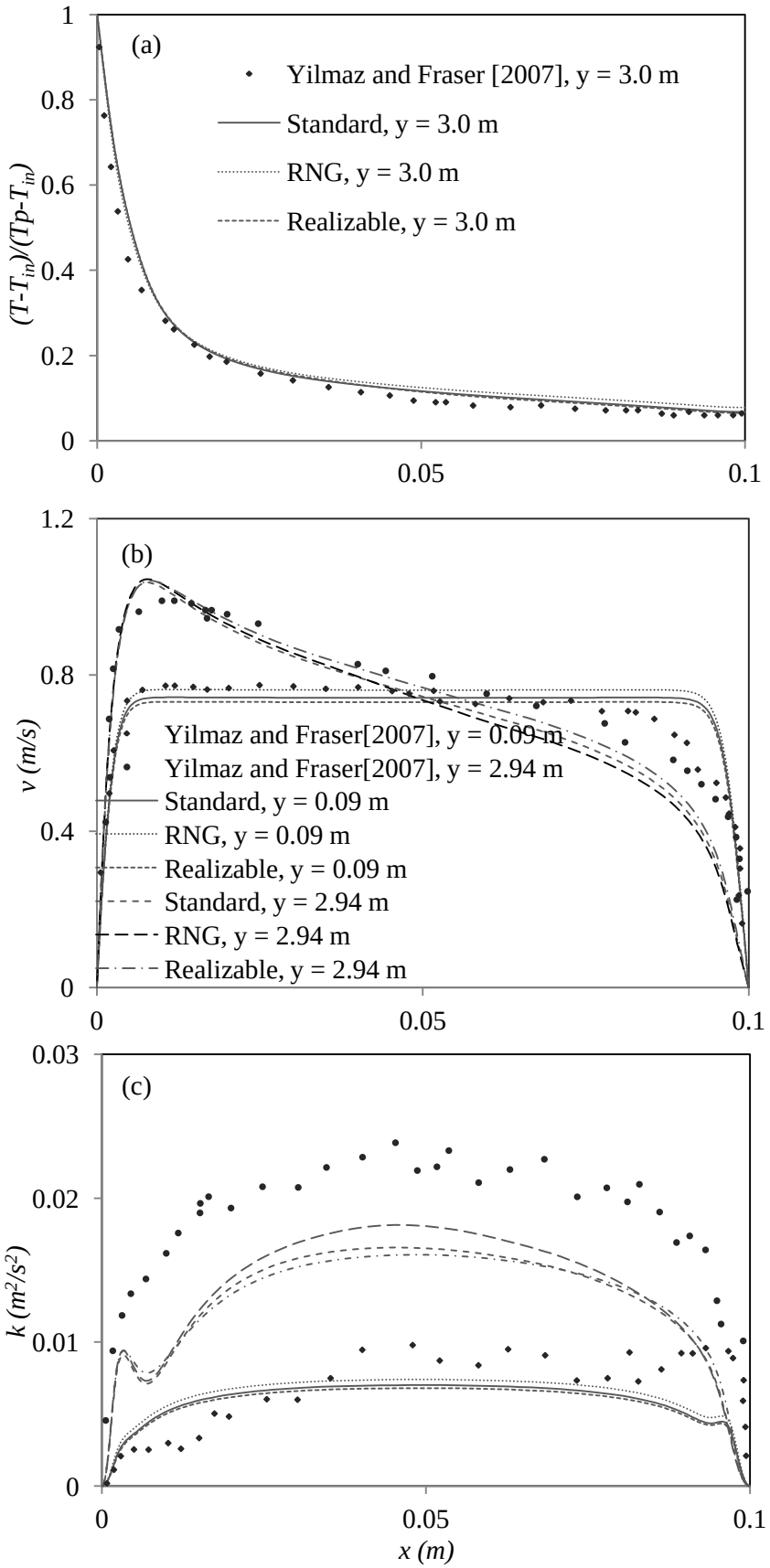

Figure 3. Outlet temperature (a), velocity (b) and turbulent kinetic energy (c).

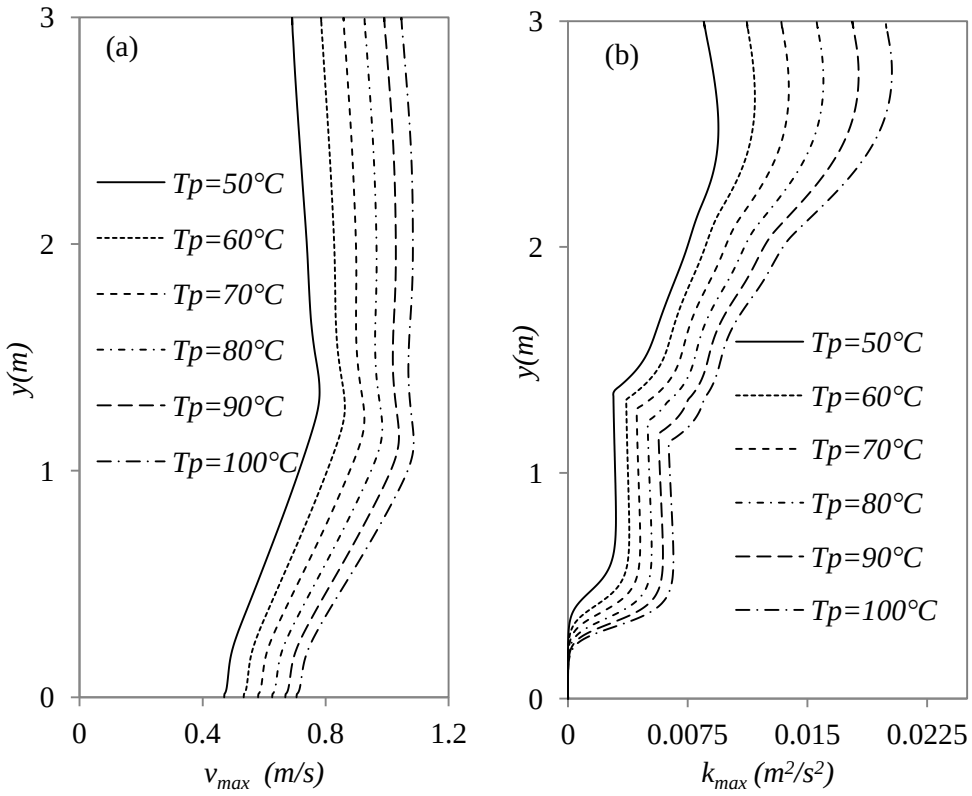

Figure 4. Distribution of the maximum velocity (a) and turbulent kinetic energy (b) at b = 0.1 m and Ta =15°C.

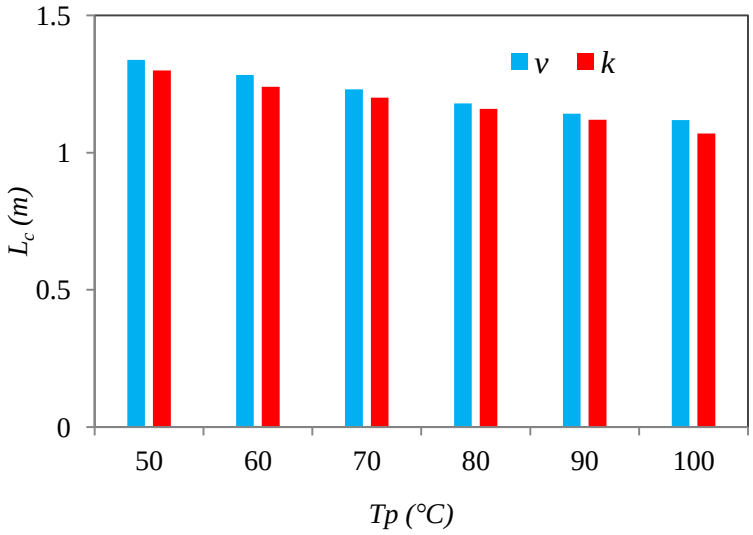

Figure 5. The critical distance derived from the velocity and kinetic energy at b = 0.1 m and Ta =15°C.

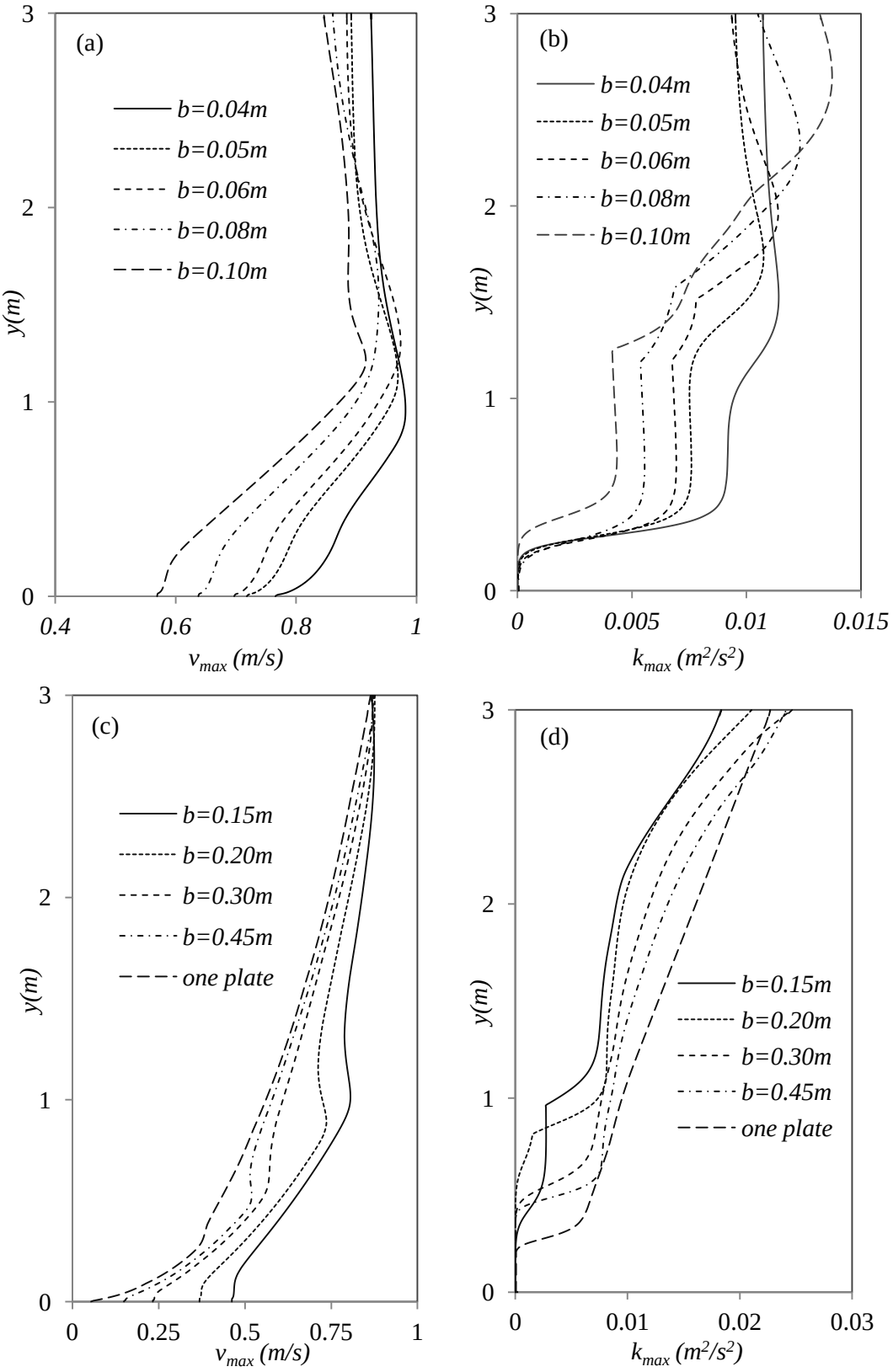

Figure 6. The distribution of the velocity (a, c) and the turbulent kinetic energy (b, d) inside the channel at *Ta* = 15°C and *Tp* =70°C.

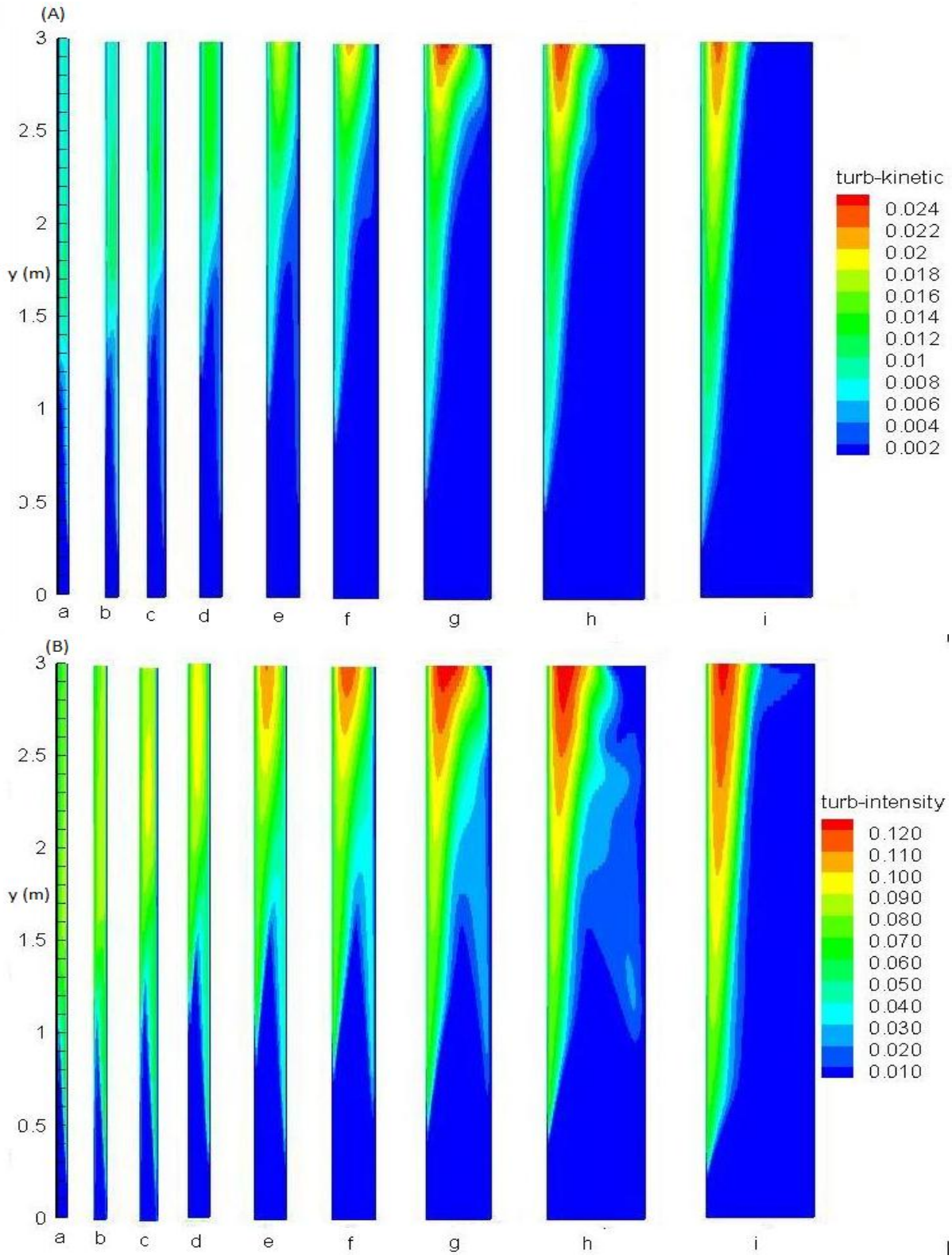

Figure 7. Contours of the turbulent kinetic energy (A) and turbulent intensity (B) for *Tp* = 70°C and *Ta* = 15°C, where the width of the channel is (a) 0.05 m, (b) 0.06 m, (c) 0.08 m, (d) 0.10 m, (e) 0.15 m, (f) 0.20 m, (g) 0.30 m and (h) 0.45 m. Note fame (i) is the one plate case.

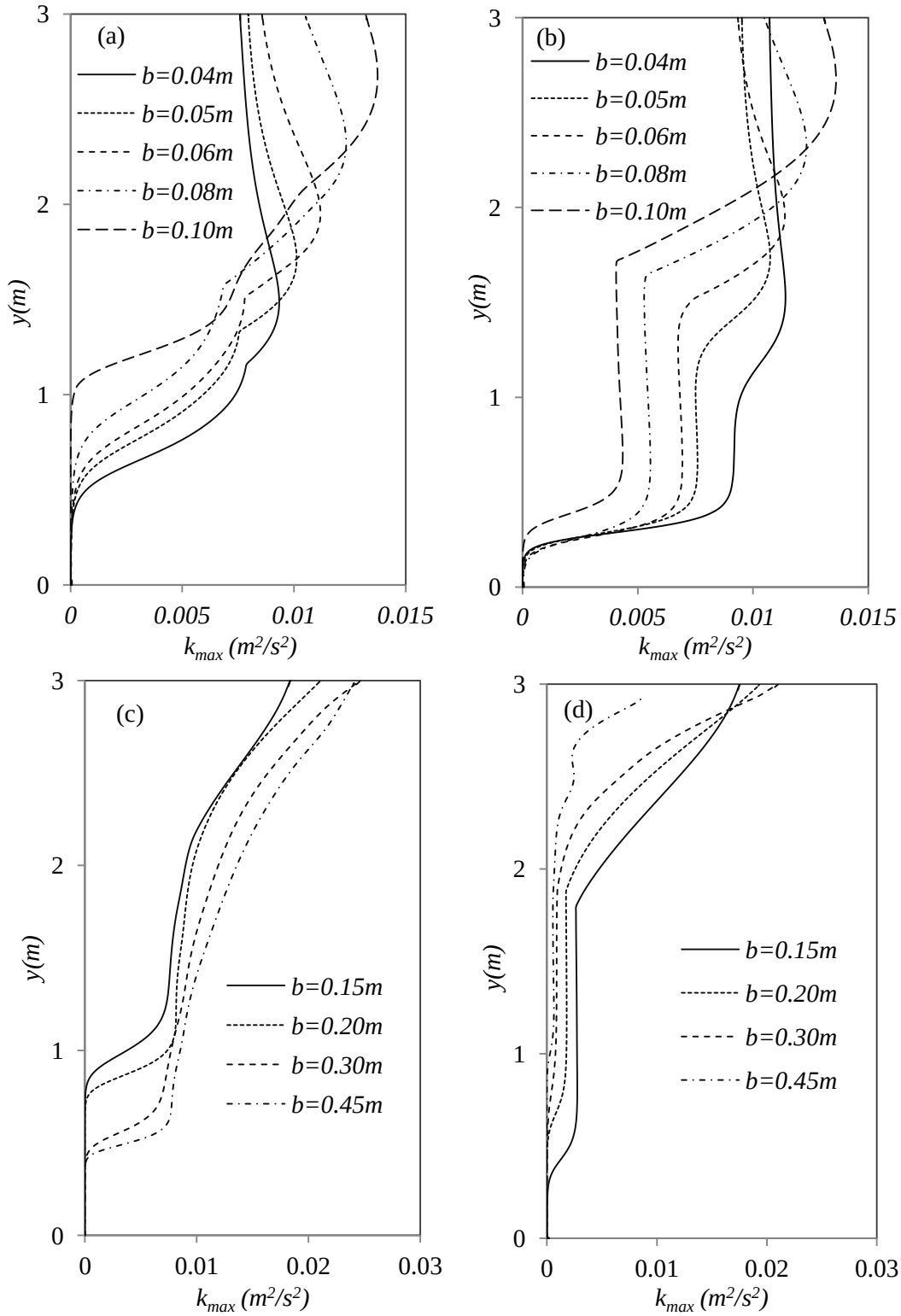

Figure 8. The distribution of the turbulent kinetic energy inside the channel at *Ta* = 15°C and *Tp* =70°C where (a, c) the left side and (b, d) the right side of the channel.

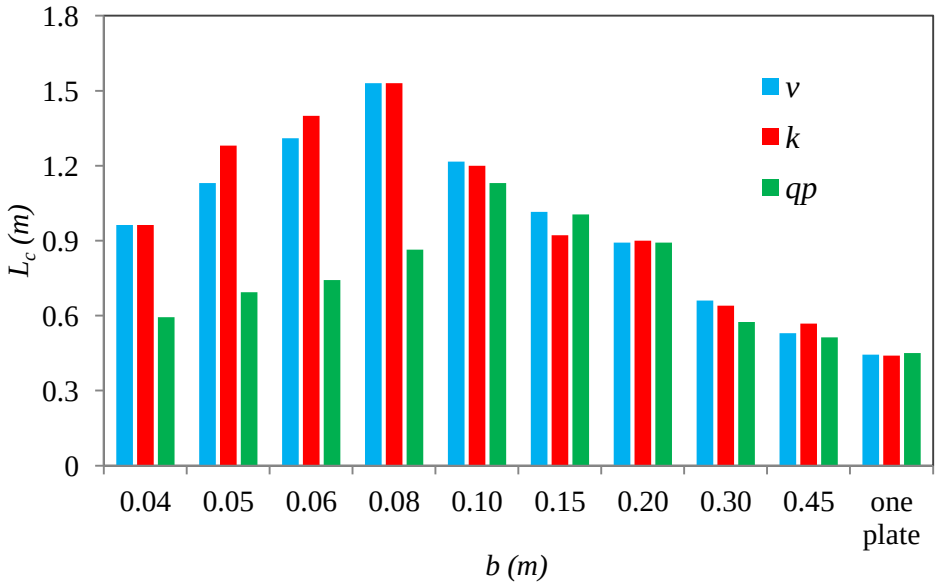

Figure 9. The critical distance derived from the velocity, kinetic energy and plate heat flux for *Tp* =70°C and *Ta* = 15°C.

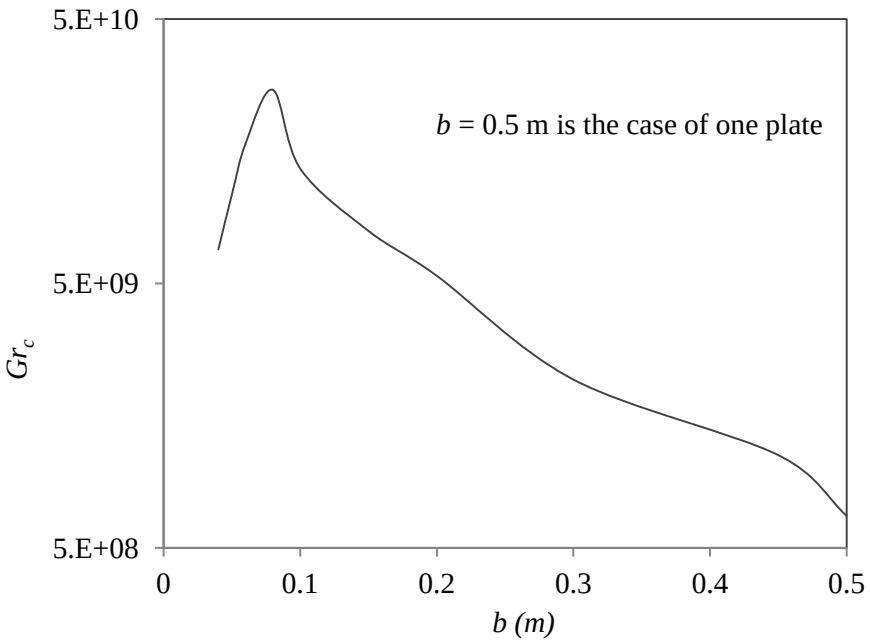

Figure 10. The Grashof number at the critical distance for *Tp* =70°C and *Ta* = 15°C.

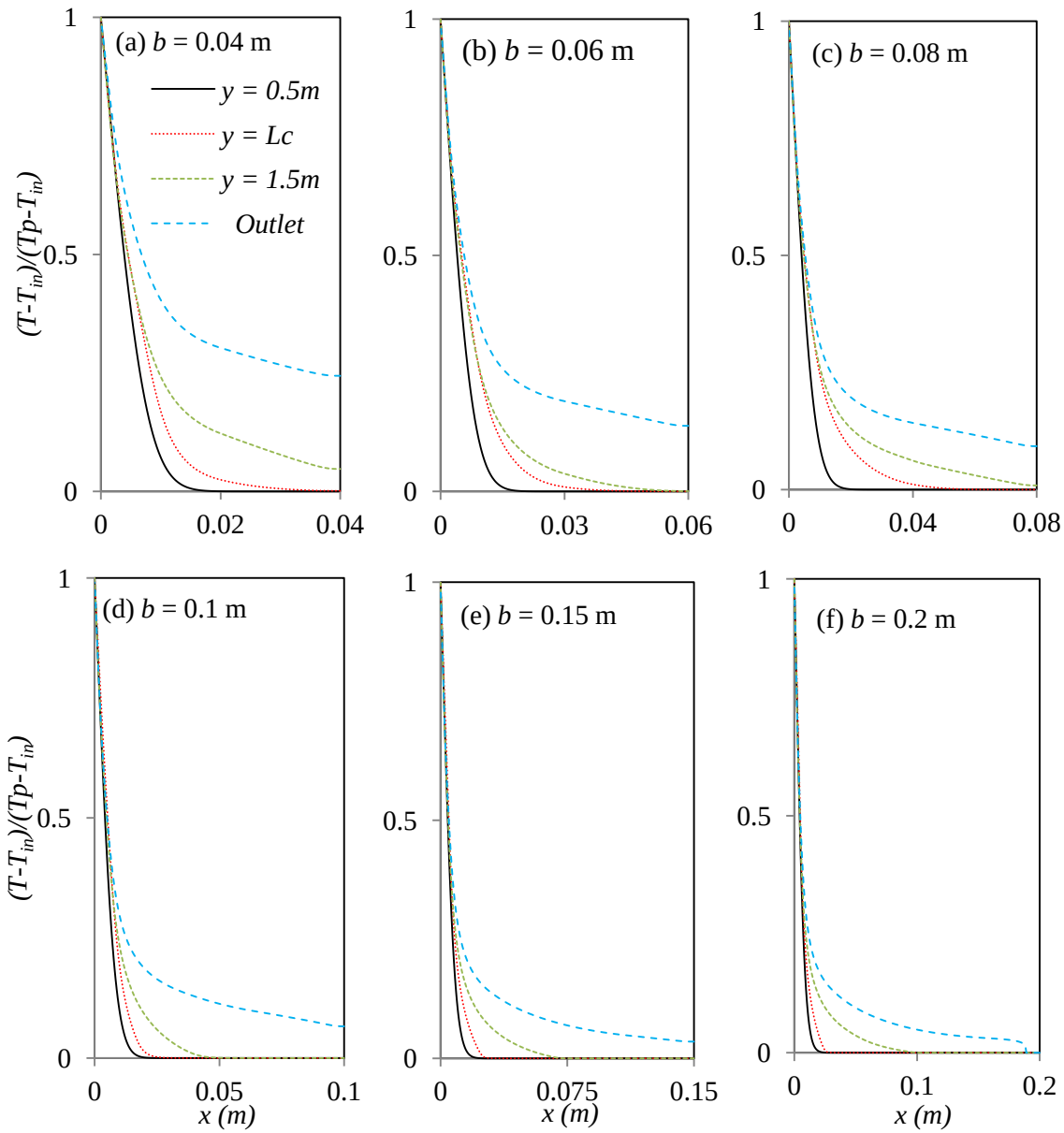

Figure 11. Distributions of the air temperature inside the channel at *Ta* = 15°C and *Tp* =70°C.

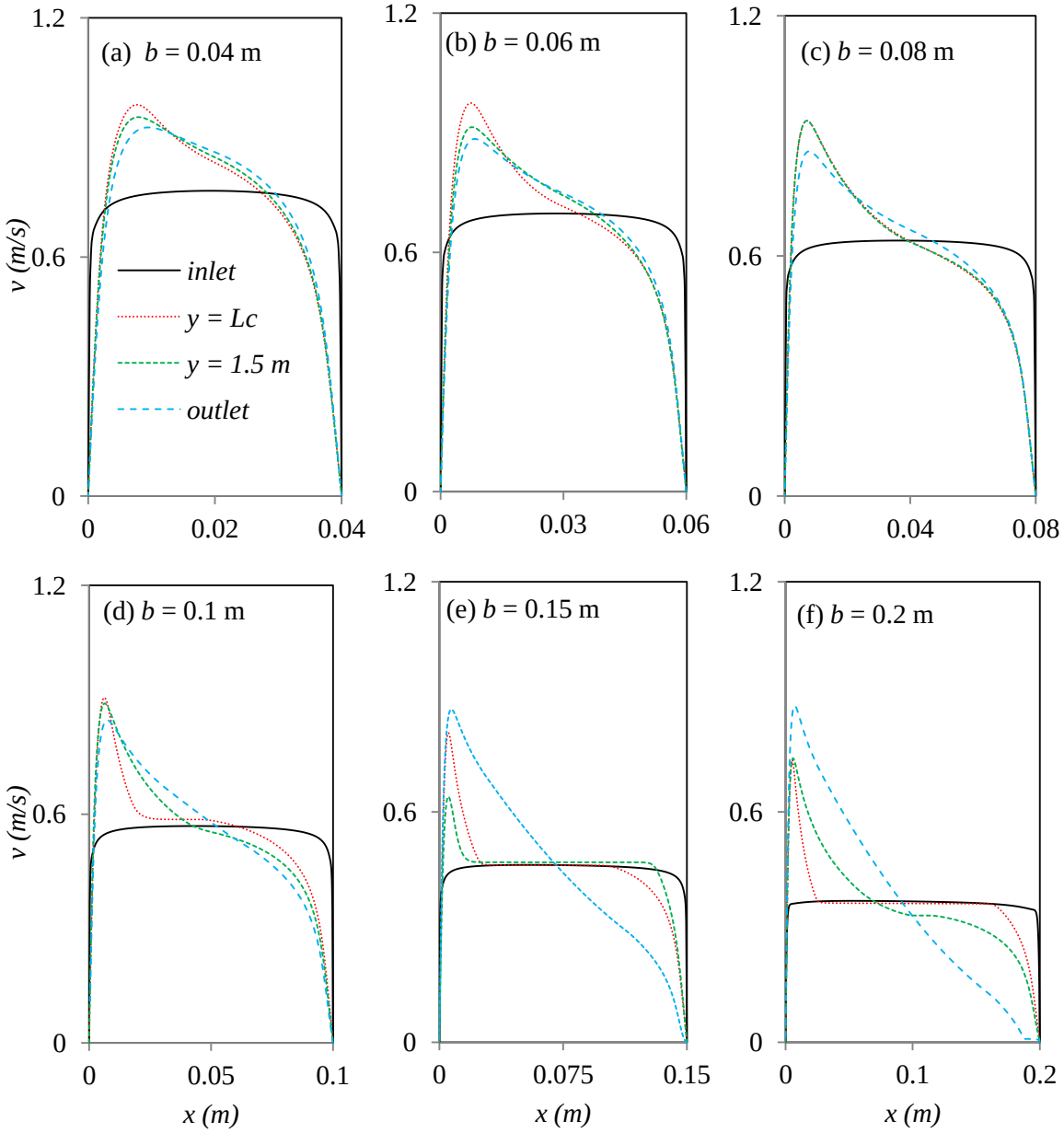

Figure 12. Distributions of the air velocity inside the channel at *Ta* = 15°C and *Tp* =70°C.

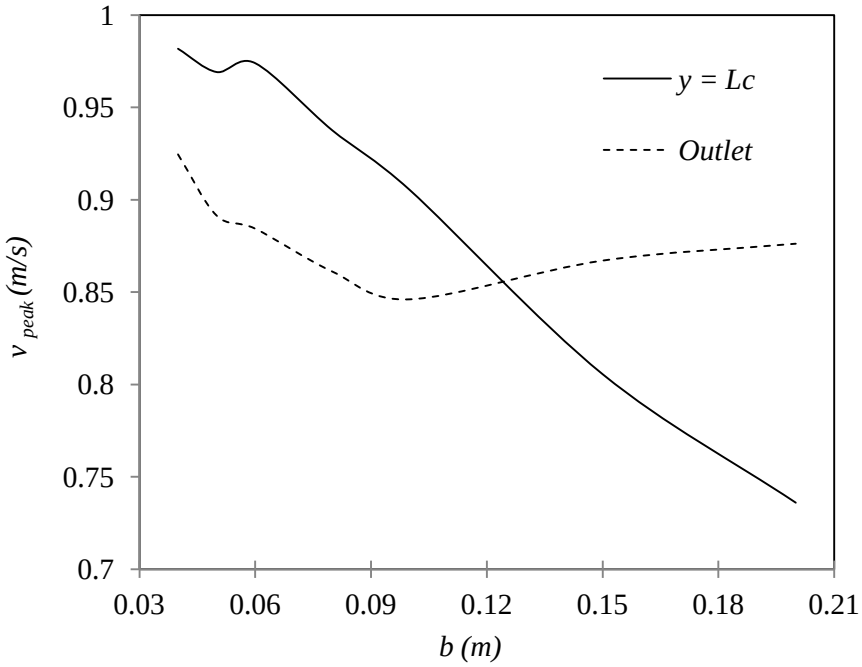

Figure 13. Comparison between the velocity peaks at the critical distance and outlet.

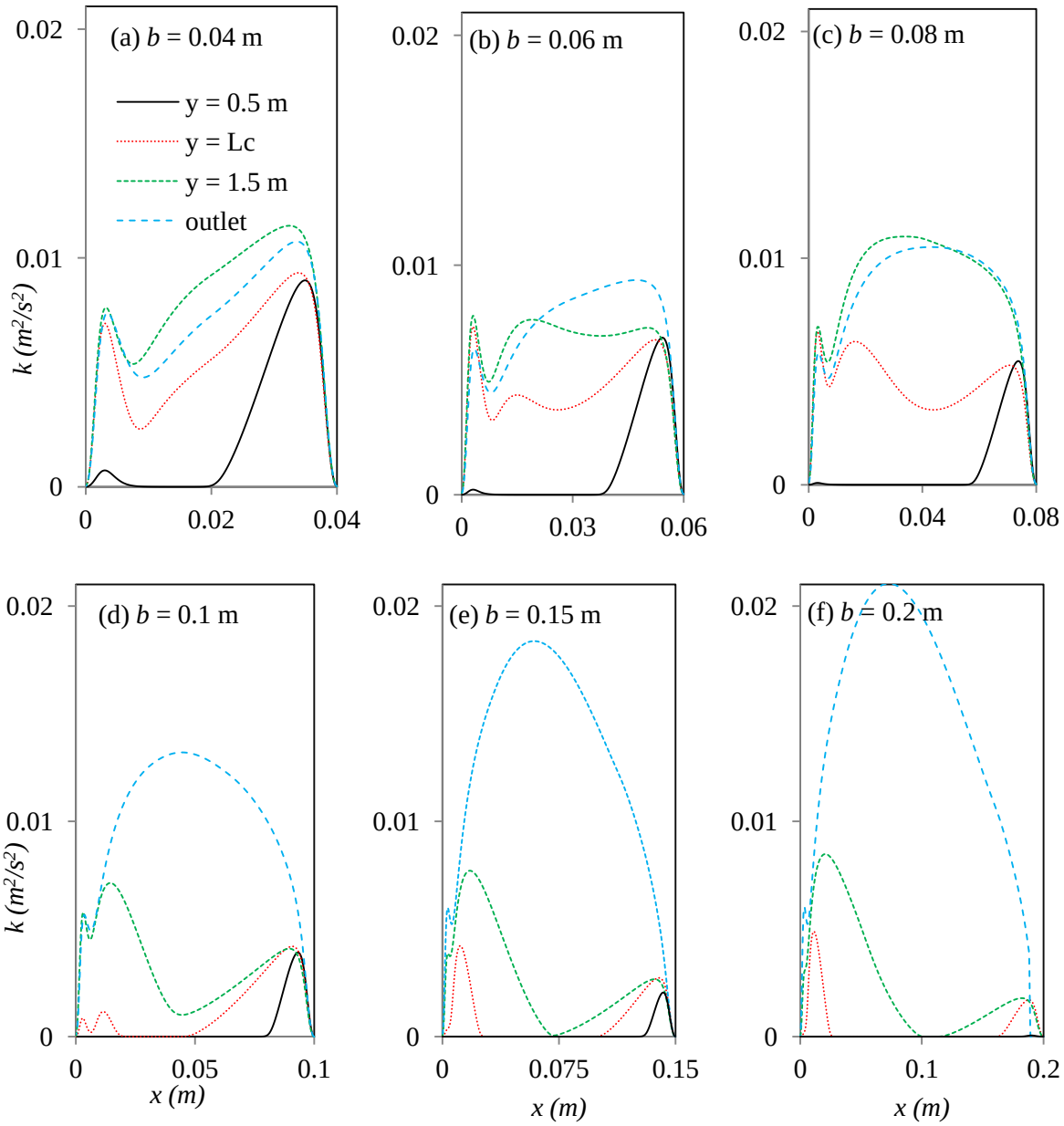

Figure 14. Distributions of the turbulent kinetic energy inside the channel at *Ta* = 15°C and *Tp* =70°C.